Structural Durability & Health Monitoring

Tech Science Press

Doi:10.32604/sdhm.2025.063813

ARTICLE

Calibration and Reliability Analysis of Eccentric Compressive Concrete Column with High Strength Rebars

Baojun Qin[1,2], **Hong Jiang**[1,2,3], **Wei Zhang**[4] **and Xiang Liu**[4,*]

[1]China Communications Construction Co., Ltd., Beijing, 100088, China
[2]China Communications Construction Corporation Rail Transit Branch, Beijing, 102200, China
[3]China Communications (Tianjin) Rail Transit Investment and Construction Co., Ltd., Tianjin, 300222, China
[4]School of Civil Engineering, Fujian University of Technology, Fuzhou, 350118, China

*Corresponding Author: Xiang Liu. Email: liuxiang@fjut.edu.cn

Received: 24 January 2025; Accepted: 23 April 2025; Published: 05 September 2025

ABSTRACT: The utilization of high-strength steel bars (HSSB) within concrete structures demonstrates significant advantages in material conservation and mechanical performance enhancement. Nevertheless, existing design codes exhibit limitations in addressing the distinct statistical characteristics of HSSB, particularly regarding strength design parameters. For instance, GB50010-2010 fails to specify design strength values for reinforcement exceeding 600 MPa, creating technical barriers for advancing HSSB implementation. This study systematically investigates the reliability of eccentric compression concrete columns reinforced with 600 MPa-grade HSSB through high-order moment method analysis. Material partial factors were calibrated against target reliability indices prescribed by GB50068-2018, incorporating critical variables including live-to-dead load ratios, design methodologies, and service conditions. The findings show that the value of k significantly affects the calibration of material partial factors, impacting the reliability of bearing capacity. Considering various k values and target reliability indices, it is recommended that the material partial factor be set at 1.15, implying that the design strength for 600 MPa high-strength steel bars should be considered as 522 MPa. For safety levels I and II, load adjustment factors of 1.1 and 0.9, respectively, may be applied.

KEYWORDS: Reliability; high-strength steel rebar; concrete column; material partial factor; high-order moment method; failure probability

1 Introduction

Recent advancements in steel manufacturing technology have enabled construction steel to achieve greater strength and ductility, resulting in high-performance materials that also contribute to material conservation in construction. Steel bars with a yield strength over 500 MPa are typically classified as high-strength steel bars (HSSB). The adoption of HSSBs could influence the mechanical properties of concrete member. Under the same reinforcement ratio, the use of HSSBs will cause a decrease in ductility, but it can reduce the reinforcement ratio to achieve the same ductility and reduce the use of materials. The price of HRB400 grade steel bars is about 5500 yuan/ton, and the price of HRB635 is about 7000 yuan/ton. The cost of HRB635 is about 27% higher than HRB400 grade, but its strength has increased by about 59%. By rational design, construction costs can be reduced.

The durability and deformation mode of HSSBs are similar to those of ordinary steel bars [1]. Consequently, researchers have explored the mechanical behavior of concrete elements containing HSSBs.

For example, Zhang et al. [2] conducted a study on the seismic performance of concrete beam—column joints that were strengthened. Luo and Li [3] examined the nonlinear behavior of concrete continuous beams with HSSBs, including their ductility and stiffness; Li et al. [4] performed eccentric loading tests on 12 circular tubed reinforced concrete columns, analyzing the effects of parameters such as the diameter to thickness ratio and load eccentricity on damage modes, load carrying capacity and ductility; Liao et al. [5] conducted an experimental study on the cyclic behavior of concrete columns with various transverse reinforcement configurations. Three designs of concrete columns with HSSBs, which included traditional closed-loop hoops, butt-welded loop hoops, and single closed-loop hoops with tie rods, were compared. Further studies on concrete members with HSSBs are listed in Table 1. These research results all indicated that HSSBs have higher yield strength and ultimate strength, and their ductility is also better than ordinary steel bars.

Table 1: Some research on RC members with HSSB

Test	Type of steel rebar	Yield strength of steel rebar	Ultimate strength of steel rebar	Elongation (%)	Citation
Concrete column under eccentric loading	Grade 600	833 MPa	1153 MPa	18	Alavi-Dehkordi and Mostofinejad [6]
Seismic behavior of concrete beam-column joint	Grade 600	824 MPa	1132 MPa	24	Alavi-Dehkordi et al. [7]
Seismic behavior of concrete column	ASTM A615 Grade 100	124 and 128 ksi	167.3 and 162 ksi	12.6 and 15.4	Aboukifa and Moustafa [8]
Seismic behavior of concrete beam-column joint	HRB600	636 and 631 MPa	773 and 813 MPa	Not provide.	Guan et al. [9]
Concrete column under axial and eccentric loading	ASTM A1035 Grade 100	810 MPa	935	Not provide.	Khalajestani et al. [10]
The static and blast response of beam	ASTM A1035 Grade 690 MPa	855 MPa	Not provide.	Not provide.	Li and Aoude [11]
Seismic behavior of concrete beam-column joint	HRB600	615 and 620 MPa	785 and 784 MPa	15 and 16	Zhang et al. [2]
Cyclic behavior of concrete column	SD685 SD785	698 MPa 886	920 MPa 1095	Not provide. Not provide.	Liao et al. [5]
Bending performance of concrete beams	HRB500	540 MPa	675 MPa	Not provide.	Zhang et al. [12]
Concrete column under eccentric loading	HRB600	701 MPa	876 MPa	20.37	Du et al. [13]

(Continued)

Table 1 (continued)

Test	Type of steel rebar	Yield strength of steel rebar	Ultimate strength of steel rebar	Elongation (%)	Citation
Concrete column under eccentric loading	HRB600	727, 737, 693 and 713 MPa	915, 932, 883 and 901 MPa	20.0, 19.5, 21.7, 21.8	Shao [14]
Cyclic behavior of flexural members	HRB400 HRB600	477 MPa 703 MPa	731 MPa 907 MPa	19 15	Hung and Chueh [15]
Cooling rates on thermos mechanically process	BST 500S	696 MPa	756 MPa	14 and 17.72	Zaky et al. [16]
The fracture behaviour of concrete prisms	Fe550	574 MPa	667 MPa	Not provide.	Krishnaa et al. [17]
Anchorage performance strength rebars	HRB600	737.36, 693.88 and 713.51 MPa	931.93, 883.04 and 901.5 MPa	19.5, 21.73 and 21.86	Xu et al. [18]
Seismic behavior of concrete columns	USD 685	961 MPa	1037 MPa	25.7	Wang et al. [19]
Seismic behavior of shear walls	HRB600	612 MPa	837 MPa	13.8	Zhang et al. [20]
Fatigue performance of steel rebars	HRB500	598	727	19	Sheng et al. [21]

When it comes to the widespread application of new construction materials in building and bridge structures, appropriate technical specifications or guidelines are essential. Regrettably, the current standards for HSSBs are lacking; they either do not exist or rely on existing guidelines, such as guideline GB50010-2010 [22], which does not specify a strength design value for steel bars with strengths above 600 MPa.

The construction process of structures inherently involves variability in material characteristics and component dimensions. Similarly, the live and dead loads that a structure bears during its operation are subject to randomness, affecting the reliability of structural safety. Consequently, modern design methods for buildings and highway bridges adopt the limit state design approach, anchored in reliability as the fundamental principle.

In reliability analysis, the simplest method entails the utilization of Monte Carlo simulation (MCS) to perform reliability assessments. Nevertheless, this method requires a considerably large quantity of samples, resulting in low analysis efficiency. Consequently, numerous researchers have explored various methods to improve reliability analysis efficiency. For example, Chen and Yang [23], as well as Li et al. [24,25], introduced a direct probability integration approach grounded in probability conservation for calculating structural reliability, and this method is characterized by its convenience, efficiency, and accuracy. Tong et al. [26] developed a fourth-order L-moments, and this method is easy to used and has applications in engineering

reliability evaluation. Zhang et al. [27,28] developed an efficient outcrossing (GLO) method based on Gauss-Legendre quadrature. The main innovations of this method are twofold: first, it evaluates the cumulative failure probability using weighted sums of outcross rates over a limited number of moments- three to five-thus avoiding the time-consuming numerical integrations that require discretization over a large number of moments. Second, it offers an efficient algorithm to calculate the outcross rate, building on the recently developed system reliability method that draws from the well-established first order reliability method (FORM). Wang et al. [29] introduced a stochastic model that integrates the physical and mechanical models, accounting for the degradation effects of crack development and corrosion progression to estimate the failure probability of reinforced concrete structures over time. Tran et al. [30] developed an effective reliability analysis program and suggested a structural resistance factor for designing a steel-concrete composite frame system consisting of steel tube concrete columns and composite beams.

Nowadays, the limit state function method is the most commonly used design method in building and bridge construction [31,32]. To assess the reliability of structural design, the partial safety factor format (PSFF) and resistance reduction factor format (RRFF) are predominantly utilized. For instance, Zhang et al. [33] analyzed the flexural strength reliability of steel-fiber reinforced plastics beams and proposed material partial factors for FRP bars in such beams. Similarly, Zhang et al. [12] investigated the flexural performance of a concrete beam incorporating HSSBs and, based on reliability theory, the bearing capacity reduction factor for the beam was proposed.

Concrete columns have traditionally been designed as principal components, with eccentric compression being one of the main force modes for columns. Columns require higher reliability compared to beams, slabs, and other components. Therefore, the reliability of the reinforced concrete (RC) column with HSSB under eccentric compression was analyzed to propose the material partial factor for HSSB, offering a theoretical foundation for for the promotion of HSSB.

2 Resistance Model for Ultimate Force of HSSBCC under Eccentric Compression

Currently, the bearing capacity design of reinforced concrete columns is **mainly applies** the limit state method, and guidelines provide specific provisions for the eccentric bearing capacity design of RC columns. The failure mode of a RC column under eccentric loading with HSSB is similar to that of with ordinary steel rebars, as shown in Fig. 1, therefore the calculation method recommended in GB50010-2010 [22] is employed.

When the length of the member is relatively long, and the second-order effect is significant due to a larger axial compression ratio in the eccentric compression member, it is essential to consider the P-δ effect in the section design. The design value for the bending moment of the eccentric compression concrete column, considering the P-δ effect, can be expressed as follows [22]:

$$M = C_{\mathrm{m}}\eta_{\mathrm{ns}}M_2 \tag{1}$$

where C_m is the eccentricity adjustment coefficient.

There are two failure mode of large eccentric compression failure or small eccentric compression failure, depending on the design scheme and loading conditions. The calculation formula for large eccentric compression failure is as follows:

$$N = \alpha_1 f_{\mathrm{c}} bx + f_y A_s - f'_y A'_s \tag{2}$$

$$Ne \le \alpha_1 f_{\mathrm{c}} bx\left(h_0 - \frac{x}{2}\right) + f'_y A'_s\left(h_0 - a'_s\right) \tag{3}$$

where $\alpha 1$ represents the coefficient, f_c denotes the standard value of concrete strength, b stands for the width of the section. Additionally, f'_y and A'_s refer to the yield strength and area of the compressive steel bar, respectively. Meanwhile f_y and A_s respectively represent the yield strength and area of the tensile steel bar. x is the height of the compression zone, e is the distance between the axial force N and the center of the resultant force of the tensile steel bar, which can be expressed as:

$$e = e_i + \frac{h}{2} - a \tag{4}$$

with

$$e_i = e_0 + e_a \tag{5}$$

where e_0 is the initial eccentricity.

The calculation formula of small eccentric compression failure is as follows:

$$N \leq \alpha_1 f_c b x + f'_y A'_s - \sigma_s A_s \tag{6}$$

$$Ne \leq \alpha_1 f_c b x \left(h_0 - \frac{x}{2}\right) + f'_y A'_s \left(h_0 - a'_s\right) \tag{7}$$

where σ_s is the stress of the tensile steel bar, which can be determined by the strain ε_s of the tensile steel bar from the assumption of the plane section, and then determined by $\sigma_s = \varepsilon_s E_s$.

(a) Tensile failure (b) Compression failure

Figure 1: Typical failure modes of RC column with HSSB under eccentric compression

3 Estimation of the Statistical Parameters of the Resistance Models

3.1 Mode Uncertainty

Structural engineering, being a blend of empirical and theoretical approaches, relies on certain fundamental assumptions for calculating the eccentric compressive capacity of RC columns. Coefficients derived from experimental data introduce uncertainties into the calculation mode, making the calculation error a stochastic variable. To ascertain the statistical characteristics of uncertainty and model error in the

calculation mode for the eccentric compressive capacity of RCCs with HSSB, 37 datasets were analyzed, as presented in Table 2. The model error μ can be expressed as [33]:

$$\mu = \frac{N_{test}}{N_{pre}} \tag{8}$$

where N_{test} and N_{pre} denote the test value and theoretical value of concrete column under eccentric compression.

Table 2: Uncertainty of calculation model

No.	Specimen	Width (mm)	Height (mm)	a_s (mm)	n	d (mm)	f_y (MPa)	f_c (MPa)	e0 (mm)	N_{test} (kN)	N_{pre} (kN)	μ	Reference
1	EC1-1	300	500	25	2	16	633	32.67	270	1779	1156	0.65	
2	EC1-2	300	500	25	2	22	633	32.67	270	2192	1705	0.78	
3	EC1-3	300	500	25	2	25	633	32.67	270	2279	1963	0.86	
4	EC3-1	300	500	25	2	16	633	32.67	220	2404	1599	0.67	
5	EC3-2	300	500	25	2	16	633	32.67	320	1289	856	0.66	Wang et al. [34]
6	EC4-1	300	500	25	2	16	633	32.67	270	1719	1156	0.67	
7	EC5-1	300	500	25	2	16	633	27.76	270	1524	1087	0.71	
8	EC5-2	300	500	25	2	22	633	27.76	270	1992	1595	0.80	
9	EC6-1	300	500	25	2	16	633	20.9	270	1364	973	0.71	
10	HRCC-1	300	400	42	2	25	540	36.1	250	1369	1292	0.94	
11	HRCC-2	300	400	42	3	25	540	36.1	250	1418	1694	1.19	
12	HRCC-3	300	400	42	2	25	540	48.1	250	1304	1409	1.08	Zhang et al. [35]
13	HRCC-4	300	400	42	3	25	540	48.1	300	1316	1469	1.12	
14	HRCC-5	300	400	42	2	25	540	36.1	300	1073	1006	0.94	
15	HRCC-6	300	400	42	3	25	540	36.1	300	1411	1370	0.97	
16	PZ1	200	350	30	2	18	700.79	33.1	100	1791	1470	0.82	
17	PZ2	200	350	30	2	18	700.79	33.1	210	1023	852	0.83	
18	PZ3	200	350	30	2	18	700.79	33.1	230	877	774	0.88	
19	PZ4	200	350	30	2	20	700.79	33.1	130	1521	1354	0.89	
20	PZ5	200	350	30	2	20	700.79	33.1	230	866	878	1.01	Du et al. [13]
21	PZ6	200	350	30	2	20	700.79	33.1	250	690	815	1.18	
22	PZ7	200	350	30	2	22	700.79	33.1	130	1560	1467	0.94	
23	PZ8	200	350	30	2	22	700.79	33.1	250	833	908	1.09	
24	PZ9	200	350	30	2	22	700.79	33.1	260	834	878	1.05	
25	HHRC-R4-Eh01	250	350	25	3	14/16	727.2	35.33	87.5	2498	1975	0.79	
26	HHRC-S4-E02	300	300	25	3	14/16	727.2	35.33	75	2401	1956	0.81	
27	HHRC-R4-Eh11	250	350	25	3	14/16	727.2	35.33	0	3632	3397	0.94	
28	HHRC-R4-Eh12	250	350	25	3	14/16	727.2	35.33	43.75	2903	2597	0.89	
29	HHRC-R4-Eh13	250	350	25	3	14/16	727.2	35.33	131.25	1885	1522	0.81	
30	HHRC-R4-Eh14	250	350	25	3	14/16	727.2	35.33	175	1559	1203	0.77	
31	HHRC-R4-Eh15	250	350	25	3	14/16	727.2	35.33	262.5	938.4	742	0.79	Shao [14]
32	HHRC-S4-E11	300	300	25	3	14/16	727.2	35.33	0	3795	3401	0.90	
33	HHRC-S4-E12	300	300	25	3	14/16	727.2	35.33	112.5	2042	1501	0.73	
34	HHRC-S4-E13	300	300	25	3	14/16	727.2	35.33	150	1608	1183	0.74	
35	HHRC-R4-Eh21	250	350	25	2	14	727.2	35.33	87.5	2126	1737	0.82	
36	HHRC-R4-Eh22	250	350	25	4	14/16	727.2	35.33	87.5	2672	2185	0.82	
37	HHRC-R4-Eh41	210	420	25	3	14/16	727.2	35.33	105	2568	2045	0.80	

The comparison between the experimental results and the theoretical estimations is illustrated in Fig. 2. Most of the results obtained by the bearing capacity calculation formulas (predicted values) are larger than the real values (test values). Among the 37 samples, only 7 samples had predicted values that were lower than the measured values. This indicates that the prediction model shows a trend of producing unsafe estimates.

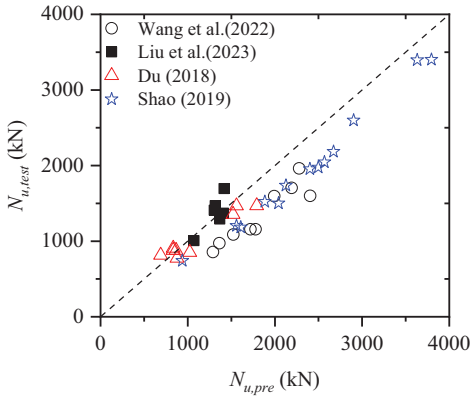

Figure 2: Comparison between predicted model calculation results and experimental results [4,14,18,34]

Fig. 3 displays the probability density function (PDF) of the model error μ, which follows a distribution with a mean value of 1.18, a standard deviation of 0.19, and a coefficient of variation of 0.16. Compared to bending components, the model for the compressive capacity of RC concrete shows more variability when using HSSB [12].

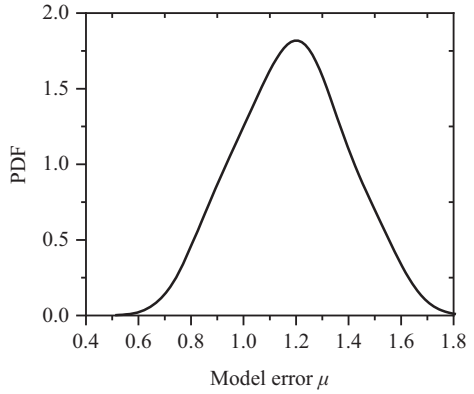

Figure 3: PDF of model error

3.2 Parameter Uncertainty

In the limit state design approach for reinforced concrete elements, the randomness primarily arises from two aspects: structural parameters and load variables. In the estimation of the eccentric compressive bearing capacity of RC columns, variables such as cross-sectional size, concrete strength, reinforcement strength, reinforcement area, eccentricity, and slenderness ratio have most influence on the bearing capacity. Thus, cross-sectional size, concrete strength, reinforcement strength, and reinforcement area are treated as random variables. For load parameters, including dead and live loads, both are also regarded as random variables. Based on the compiled data in Table 2, the yield strength bias of HSSB is 1.17, with a coefficient of variation of 0.096. The statistical details for each random variable are provided in Table 3.

Table 3: Statistical characteristics of random variables

Random variable	Bias	COV	Distribution	Reference
Section width/section height	1.00	0.02	Normal	Lu et al. [36]
Strength of concrete	1.15	0.15	Lognormal	Ribeiro and Diniz [37]
Area of reinforcement	1.00	0.03	Normal	Lu et al. [36]
Dead load	1.06	0.075	Normal	GB50068-2018 [38]
Live load (house)	0.644	0.233	Extreme type I	GB50068-2018 [38]
Dead load (office)	0.524	0.288	Extreme type I	GB50068-2018 [38]

4 Reliability Theory

4.1 Statistical Moment Calculation

Suppose p(x) denotes the probability density function of a continuous random variable $Y = G(\mathbf{X})$. As defined in [39], its mean value M_1 and k-th central moments M_k are expressed as follows:

$$M_1 = E\left[G\left(\mathbf{X}\right)\right] = \int_{-\infty}^{\infty} G\left(\mathbf{X}\right) p\left(\mathbf{X}\right) d\mathbf{X} \tag{9}$$

$$M_k = \int_{-\infty}^{\infty} \left[G\left(\mathbf{X}\right) - \mu\right]^k p\left(\mathbf{X}\right) d\mathbf{X} \text{ fork} \geq 2 \tag{10}$$

As the random variable Y includes multiple variables, the statistical moments of $G(\mathbf{X})$ cannot be acquired directly. In such instances, dimensionality reduction is performed as described in Rahman and Xu [40]. When a function contains n random variables, it can be resolved into s-dimensional random variable functions $G^s(X)$, as shown below:

$$G\left(\mathbf{X}\right) \cong G^s\left(\mathbf{X}\right) = \sum_{i=0}^{s} \left(-1\right)^i C_{n-s+i-1}^{i} \sum_{k_1 < \cdots < k_{s-i}} y_{s-i} \tag{11}$$

where $s < n$, and $y_{s-i} = G\left(c_1, \cdots, c_{k_1-1}, x_{k_1}, c_{k_4+1}, \cdots, c_{k_{c-1}-1}, x_{k_{c-i}}, c_{k_{c-1}+1}, \cdots, c_n\right)$; c is a reference point, and it equals to $\left[c_1, \quad c_1, \quad \cdots \quad c_n\right]$.

When s = 2, the multivariate function problem is transformed into a problem of combining multiple univariate functions, and then Eq. (14) transform to the following formula:

$$g\left(\mathbf{X}\right) \cong g^1\left(\mathbf{X}\right) = \sum_{i=1}^{n} g_i\left(X_i\right) - \left(n-1\right) g\left(c\right) \tag{12}$$

with

$$g_i\left(\mathbf{X}_i\right) = g\left(c_1, \cdots, c_{i-1}, X_i, c_{i+1}, \cdots, c_n\right) \tag{13}$$

This indicates that except the i-th variable, all other variables maintain their corresponding values at the reference point.

Through the substituting Eq. (15) into Eqs. (12) and (13), the statistical moment of the dimensionality reduced random variable Y can be obtained as follows:

$$\mu = E\left[\sum_{i=1}^{n} g_i\left(X_i\right) - \left(n-1\right) g\left(c\right)\right] \cong \sum_{i=1}^{n} E\left[g_i\left(X_i\right)\right] - \left(n-1\right) g\left(c\right) \tag{14}$$

$$M_z \cong E\left[\sum_{i=1}^{n}\left(g_i-\mu\right)^z-(n-1)\left[g\left(c\right)-\mu\right]^z\right]$$
$$=\sum_{i=1}^{n}E\left\{\left[g_i\left(X_i\right)-\mu\right]^z\right\}-(n-1)\left[g\left(c\right)-\mu\right]^z\left(z=2,3,4\right) \tag{15}$$

When the random variables in $G(X)$ follow a normal distribution, $E\left[g_i\left(X_i\right)\right]$ and $E\left\{\left[g_i\left(X_i\right)-\mu\right]^z\right\}$ can be evaluated through Gaussian-Hermite integration and expressed as:

$$E\left[g_i\left(X_i\right)\right]=\sum_{l=1}^{r}\frac{w_{\mathrm{GH},l}}{\sqrt{\pi}}g_i\left(\sqrt{2}x_{\mathrm{GH},l}\right) \tag{16}$$

$$E\left[\left(g\left(X_i\right)-\mu\right)^z\right]=\sum_{l=1}^{r}\frac{w_{\mathrm{GH},l}}{\sqrt{\pi}}\left[g_i\left(\sqrt{2}x_{\mathrm{GH},l}\right)-\mu\right]^z \tag{17}$$

where r represents the number of integration point; $x_{GH,l}$ and $w_{GH,l}$ denote the integration point and the weight of Gaussian-Hermite, respectively, with detailed values available in references.

For s = 2, the multivariate function problem reduces to combining univariate functions, and then Eq. (14) transform to the following formula [39]:

$$M_1\approx\sum_{l<m}E\left[g\left(X_l,X_m,u_c\right)\right]-(n-2)\sum_{k=1}^{n}E\left[g\left(X_k,u_c\right)\right]+\frac{(n-1)(n-2)}{2}g\left(u_c\right) \tag{18}$$

$$M_z\approx\sum_{l<m}E\left[\left(g\left(X_l,X_m,u_c\right)-\mu_s\right)^z\right]-(n-2)\sum_{k=1}^{n}E\left[\left(g\left(X_k,u_c\right)-\mu_s\right)^z\right]$$
$$+\frac{(n-1)(n-2)}{2}\left(g\left(u_c\right)-\mu_s\right)^z\left(z=2,3,4\right) \tag{19}$$

$$\begin{cases}\mu_s=M_1\\ \sigma_s=\sqrt{M_2}\\ \alpha_{3G}=M_3/{\sigma_s}^3\\ \alpha_{4G}=M_4/{\sigma_s}^4\end{cases} \tag{20}$$

where M_z denotes the z-th central moment; α_3 and α_4 respectively stand for the skewness coefficient and the kurtosis coefficien; $g(u_c)$ denotes the response value under the condition that all random parameters take values corresponding to the reference point; $g(X_k, u_c)$ denotes response value when k-th parameter is considered as random variable while the others are set to their reference values; $g(X_l, X_m, u_c)$ denotes response value when l-th and m-th parameters are considered as random variable while the others are corresponding to the reference point. $E\left[\left(g\left(X_k,u_c\right)-\mu_s\right)^z\right]$ and $E\left[\left(g\left(X_l,X_m,u_c\right)-\mu_s\right)^z\right]$ can be calculated based on Gaussian Hermite integration, and they can be formulated in the following functions:

$$E\left[\left(g\left(X_k,u_c\right)-\mu_s\right)^z\right]=\sum_{i=1}^{h}\frac{w_{GH,i}}{\sqrt{\pi}}\left(g\left(\sqrt{2}x_{k,i},u_c\right)-\mu_s\right)^z \tag{21}$$

$$E\left[\left(g\left(X_l,X_m,u_c\right)-\mu_s\right)^z\right]=\sum_{i=1}^{h}\sum_{j=1}^{h}\frac{w_{GH,i}w_{GH,j}}{\pi}\left(g\left(\sqrt{2}x_{l,i},\sqrt{2}x_{m,j},u_c\right)-\mu_s\right)^z \tag{22}$$

4.2 Calculation of Reliability Index

The failure probability P_f can be expressed as a function of the fourth order moment reliability index β_{4M} function based on the center moment of the first four moments of the limit state function, and it can be written as [39]:

$$P_f = \Phi(-\beta_{4M}) \tag{23}$$

where $\Phi(\cdot)$ represents the cumulative distribution function for the standard normal distribution, and the detail calculation formula of β_{4M} can be found in Zhao and Lu [39], and this method can also be termed high order moment method (HOMM).

4.3 LimitStateFunction

Before analyzing the reliability of the structure, a limit state function is neccessary to be established, and its fundamental expression is presented below:

$$Z = \mu R - \gamma_G S_{Gk} - \gamma_Q S_{Qk} \tag{24}$$

where R is resistance, and it can satisfy Eqs. (1)–(10); γ_G and γ_Q represents the partial factor of dead load and live load, respectively; S_{Gk} and S_{Qk} respectively represents the standard values of dead load and live load, and they can be given as follows:

$$\begin{cases} S_{Gk} = \frac{S_d}{\gamma_G + k\gamma_Q} \\ S_{Qk} = \frac{kS_d}{\gamma_G + k\gamma_Q} \end{cases} \tag{25}$$

where S_d is the standard value of load, and k denotes the ratio of live load to dead load.

5 Analysis of Reliability and Partial Factor

According to Eqs. (1) to (7), the prediction value of the bearing capacity of eccentrically compressed RC columns with HSSBs can be determined, and the moment values of limit state function can be calculated by Eqs. (14) to (22) and Eqs. (24) and (25). Then the reliability index and failure probability can be obtained by Eq. (23).

5.1 Reliability Analysis

The precision of the methods used for reliability calculations plays a significant role in the dependability of reliability analysis. Considering six cross-sections as examples, presented in Table 4, the reliability of RC cross-sections under eccentric loads was calculated using the HOMM, and these results are compared with those obtained from the Monte Carlo simulation (MCS) method. While MCS is a straightforward and precise method for reliability calculations, it necessitates a significant sample size for accurate outcomes. Moreover, this section will explore the material partial factors for HSSB, the value of k, and how varying load conditions (house load or office) affect the reliability indexes.

Table 4: Case of reliability analysis

No.	Specimen	Width (mm)	Height (mm)	a_s (mm)	n	d (mm)	f_c (MPa)	e_0 (mm)
1	EC1-1	300	500	25	2	16	32.67	270
2	EC1-2	300	500	25	2	22	32.67	270

(Continued)

Table 4 (continued)

No.	Specimen	Width (mm)	Height (mm)	a_s (mm)	n	d (mm)	f_c (MPa)	e_0 (mm)
3	EC1-3	300	500	25	2	25	32.67	270
4	EC3-1	300	500	25	2	16	32.67	220
5	EC3-2	300	500	25	2	16	32.67	320
6	EC4-1	300	500	25	2	16	32.67	270

The reliability indices computed by HOMM and MCS are displayed in Fig. 4. It is evident that the reliability indices from HOMM are in agreement with those from MCS, affirming the method's accuracy. Furthermore, it is observed that for different design sections, the reliability index exhibits a linear increase with the rise in material partial factors, and this is because the increase in partial factor leads to a greater actual bearing capacity, which is consistent with the results in the literatures [41,42].

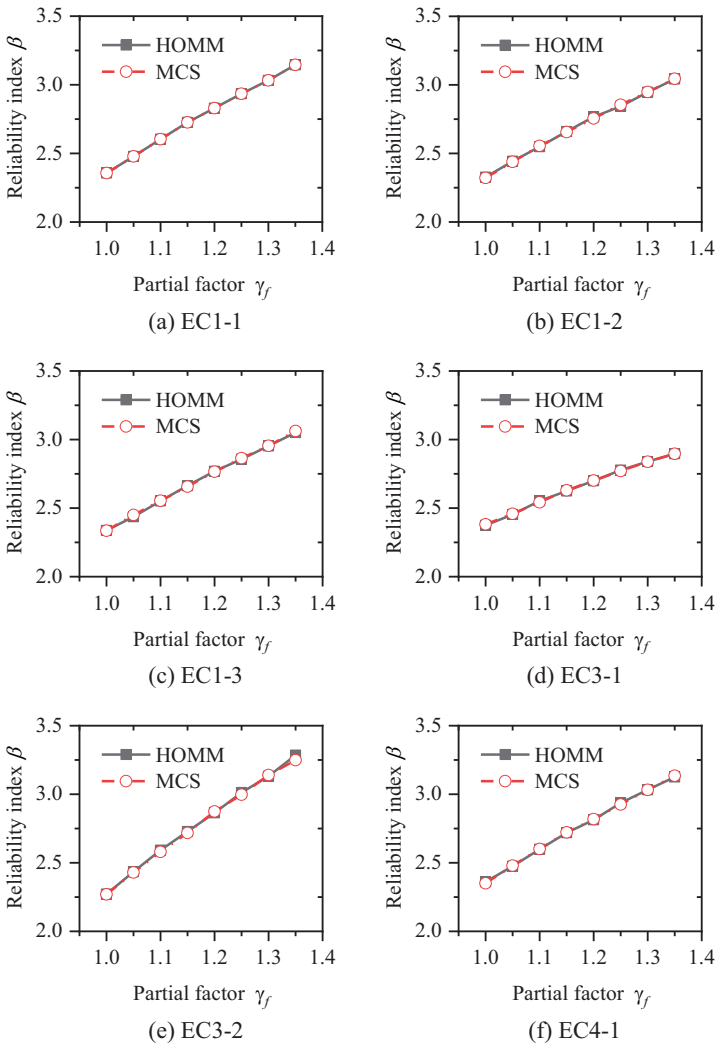

Figure 4: Calculation result from HOMM and MCS

Fig. 5 illustrates the reliability indices for varying k values and material partial factors, considering both house load and office loads. In different scenarios, the reliability index similarly shows a linear upward trend with the increase in material partial factors. Additionally, the reliability index increases with higher k values, indicating that the distribution ratio of lateral to live load in the design significantly influences reliability.

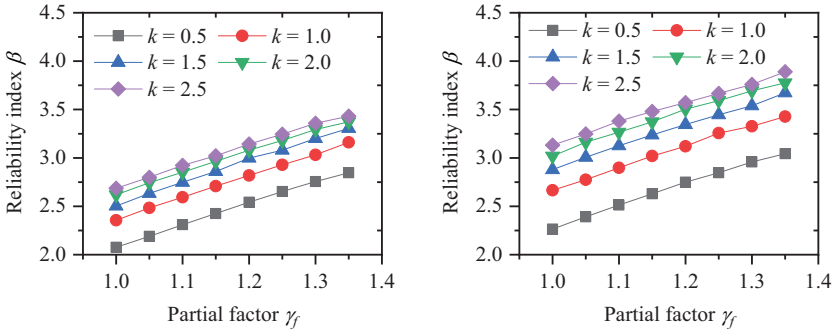

Figure 5: Reliability indexes under various k values

5.2 Calibration of Material Partial Factor

Structural safety and economy are often seen as conflicting factors in design. A high reliability index may lead to an excessive structural surplus, indicating a compromise in economic efficiency. Conversely, a low reliability index may risk structural safety. Design guidelines often differentiate target reliability indices based on the importance level of the results, as specified in GB5068-2018 [38], which is detailed in Table 5.

Table 5: Target reliability index

	Level I	Level II	Level III
Brittle comment	4.2	3.7	3.2
Ductile comment	3.7	3.2	2.7

To determine the optimal material partial factors, multiple eccentrically loaded RC rectangular sections were designed, with parameters listed in Table 6. These parameters encompass five section widths, seven section heights, four concrete strength classes, ten eccentricities, and eight reinforcement ratios, yielding a total of 5 × 7 × 4 × 10 × 8 = 11,200 cases. For each set of parameters under identical conditions, a reliability index is calculated, resulting in 11,200 reliability indices. To calibrate the material partial factors, the following index can be utilized [33]:

$$H = \frac{1}{n}\sum_{i=1}^{n}(\beta_i - \beta_T) \tag{26}$$

where β_i and β_T represents the calculated reliability index and the target reliability index, respectively, and the value of β_T can be found in Table 5; n represents the number of calculated cases. As the calibration value decreases, the reliability index associated with the material partial factor progressively converges toward the target reliability index, and its value is more reasonable.

Table 6: Design parameters

Parameter	Unit	Range	Interval
Width b	mm	300 to 500	50
Height h	mm	300 to 600	50
Concrete strength fc	MPa	16.7, 20.1, 23.4, 26.8	–
Type of reinforcement	–	–	–
Eccentricity e_0	mm	50 to 500	50
Reinforcement ratio ρ_s	%	0.5 to 2.0	0.2

Separate assessments for house and office loading conditions were conducted to ascertain the optimal material partial factor, with these factors ranging from 1.0 to 1.35 at increments of 0.05. The considered k values were 0.5, 1.0, 1.5, 2.0, and 2.5. The calibration results are presented in Figs. 6 and 7.

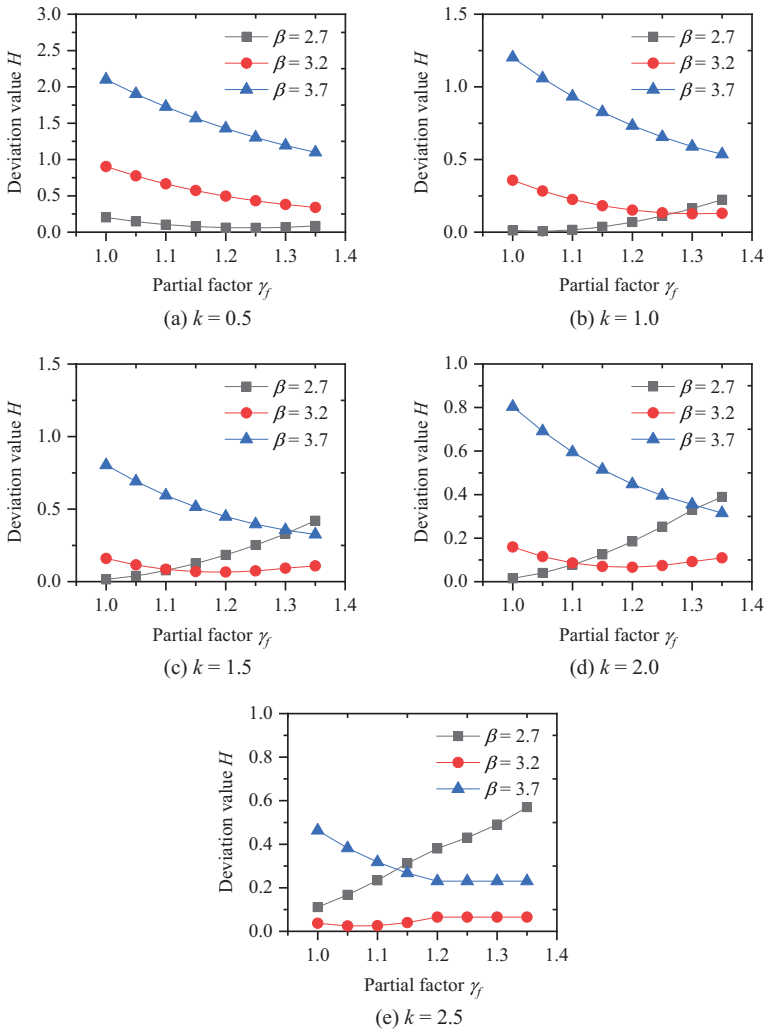

Figure 6: Calibration for partial factor of office condition

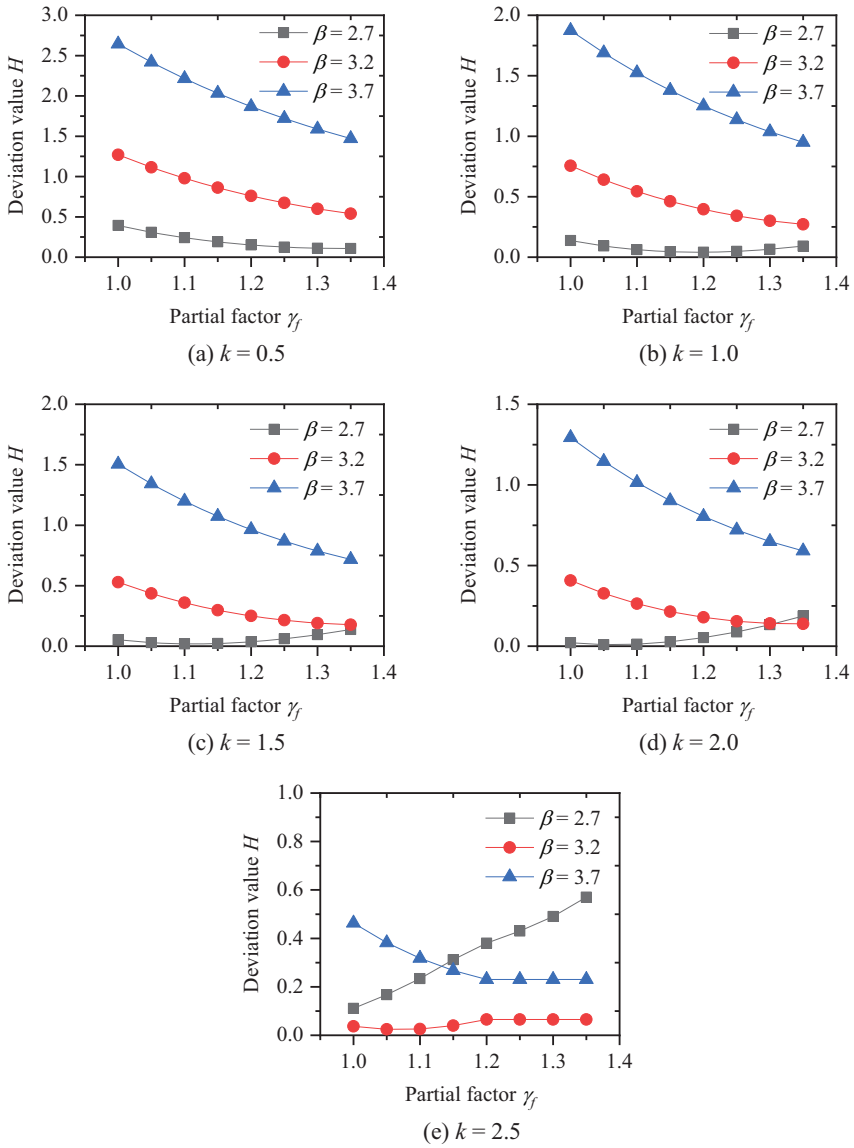

Figure 7: Calibration for partial factor of house condition

According to Fig. 6, the value of k significantly influences the calibration of reliability indices. At k = 0.5, the calibration values for target reliabilities of 3.2 and 3.7 decrease with increasing material partial factors, while for a target reliability of 2.7, the calibration values initially decrease and then increase, with the lowest value occurring at approximately 1.15. At k = 1.0, the calibration values for target reliabilities of 3.2 and 3.7 decrease with increasing material partial factors, whereas for a target reliability of 2.7, they increase with increasing material partial factors. At k = 1.5, the calibration value for a target reliability of 3.2 initially declines and then rises with a rise in the material partial factor, reaching its minimum at around 1.18. For a target reliability of 2.7, the calibration value increases, while for a target reliability of 3.7, it decreases with increasing material partial factor. At k = 2.0 and 2.5, the calibration values of the reliability indices are similar to those observed at k = 1.5.

Fig. 7 shows the situation for house loading. Similarly, the value of k has a significant impact on the calibration of reliability indices. At k = 0.5, the calibration values of different target reliabilities increase with

the material partial factor. At k = 1.0, the calibration values for target reliabilities of 3.2 and 3.7 decrease with increasing material partial factors, while those for a target reliability of 2.7 initially decrease and then increase, with the lowest value occurring at approximately 1.15. At k = 1.5, the calibration value for a target reliability of 3.2 shows a similar pattern of initial decrease and subsequent increase, with the lowest value at around 1.18. For a target reliability of 2.7, the calibration value increases, while for a target reliability of 3.7, it decreases with increasing material partial factors. At k = 2.0 and 2.5, the calibration values follow the pattern observed at k = 1.5.

Based on the calculations, it is recommended to set the material partial factor at 1.15 for a target reliability index of 3.2. For cases with reliability indices of 2.7 and 3.7, it is advisable to refer to the specifications and apply load effect amplification factors of 0.9 and 1.1, respectively. According to the material partial factor, the strength design value of corresponding high-strength reinforcement can be obtained as shown in Table 7.

Table 7: Design strength of steel rebar

Grade	Standard strength (MPa)	Design strength (MPa)	Note
HRB335	335	300	GB50010-2010
HRB400	400	360	GB50010-2010
HRB500	500	435	GB50010-2010 and proposed
HRB600	600	520	Proposed

6 Discussions

(1) HOMM has high accuracy and computational efficiency in calculating reliability indexes, and it is easy to use, and it can be widely applied in reliability analysis of other types of concrete structures.

(2) The material partial factor of HRB335 and HRB400 in the code GB50010-2010 is about 1.11, and their strength design values are 300 and 360 MPa, respectively; Regarding axial compressive strength, the compressive strength design value for HRB500 and HRBF500 reinforcement is 400 MPa, with a partial factor of 1.25. Conversely, other cases have a design strength of 435 MPa and a partial factor of 1.15. These results are in line with those presented in this paper, though the 1.25 partial factor is viewed as quite conservative. For reinforcement with standard tensile strength of 600 MPa, the recommended strength design value is 520 MPa, as shown in Table 7.

(3) It is important to mention that the proposed partial factors for HSSB were derived from the bearing capacity of eccentrically compressed RC columns. Additional investigations are required to verify whether member under other states are also applicable.

(4) The coefficient of variation of high-performance steel bars is inconsistent with that of ordinary steel bars, resulting in inconsistent partial factor. This research provides some reference for the calibration strategy of partial factor for other high-performance materials.

7 Conclusions

To enhance the application of HSSB concrete, this study addressed the uncertainty in the approach used to determine the load-bearing capacity of RC columns with HSSB under eccentric compression. The uncertainties of other parameters were also collected. A limit state function was formulated, taking into account various ratios of dead load to live load. The HOMM was employed to evaluate the reliability of the bearing capacity of reinforced concrete columns under eccentric compression, and its accuracy was validated. Extensive case studies were conducted to determine the calibration values for material partial factors under

different dead-to-live load ratios and usage conditions, leading to the identification of optimal factors. The main conclusions are as follows:

(1) For RC columns with HSSB under eccentric compression, the calculation method's uncertainty is represented by a normal distribution, with parameters including a mean of 1.18, a standard deviation of 0.19, and a coefficient of variation of 0.16.

(2) The HOMM has proven to be both efficient and accurate in calculating the reliability of the bearing capacity for eccentrically compressed RC columns with HSSB when compared to MCS.

(3) The reliability of the bearing capacity of reinforced concrete columns is greatly affected by the ratio of dead load to live load. As this ratio rises, the reliability index typically becomes higher. Additionally, an increase in the material partial factor leads to a linear increase in the reliability index.

(4) Based on the computational results, it is advised that the material partial factor be set according to a target reliability index of 3.2, which is recommended to be 1.15. For cases with reliability indices of 2.7 and 3.7, it is appropriate to consult the specifications and apply load effect amplification factors of 0.9 and 1.1, respectively.

Acknowledgement: Not applicable.

Funding Statement: The work described in this paper is supported by grants from the Natural Science Foundation of Fujian Province (Grant No. 2022J05184).

Author Contributions: Baojun Qin: Performed the review, wrote the manuscript. Hong Jiang: Detailed check of the text and references, editorial contribution. Wei Zhang: Detailed check of the text and references, editorial contribution. Xiang Liu: Planned and organized the paper, performed the review, wrote the manuscript, performed editorial tasks, organized the tasks, served as a corresponding author. All authors reviewed the results and approved the final version of the manuscript.

Availability of Data and Materials: Available upon request.

Ethics Approval: Not applicable.

Conflicts of Interest: The authors declare no conflicts of interest to report regarding the present study.

References

1. Xiao Z, Wei H, Wu T, Ren W, Li X. Flexural behavior and serviceability of steel fiber-reinforced lightweight aggregate concrete beams reinforced with high-strength steel bars. Constr Build Mater. 2024;437(8):136977. doi:10.1016/j.conbuildmat.2024.136977.
2. Zhang X, Rong X, Shi X, Zhang J. Experimental evaluation on the seismic performance of high-strength reinforcement beam-column joints with different parameters. Structures. 2023;51(6):1591–608. doi:10.1016/j.istruc.2023.03.100.
3. Luo D, Li B. Moment redistribution capacity of continuous RC beams with High-Strength steel reinforcement. Structures. 2023;51(5):13–24. doi:10.1016/j.istruc.2023.03.005.
4. Li X, Liu J, Wang X, Chen YF. Behavior of eccentrically-loaded tubed reinforced concrete short columns with high-strength concrete and reinforcement. Constr Build Mater. 2023;378(4):131148. doi:10.1016/j.conbuildmat.2023.131148.
5. Liao WC, Perceka W, Wang M. Experimental study of cyclic behavior of high-strength reinforced concrete columns with different transverse reinforcement detailing configurations. Eng Struct. 2017;153(1):290–301. doi:10.1016/j.engstruct.2017.10.011.
6. Alavi-Dehkordi S, Mostofinejad D. Behavior of concrete columns reinforced with high-strength steel rebars under eccentric loading. Mater Struct. 2018;51(6):145. doi:10.1617/s11527-018-1271-3.

7. Alavi-Dehkordi S, Mostofinejad D, Alaee P. Effects of high-strength reinforcing bars and concrete on seismic behavior of RC beam-column joints. Eng Struct. 2019;183(1):702–19. doi:10.1016/j.engstruct.2019.01.019.
8. Aboukifa M, Moustafa MA. Experimental seismic behavior of ultra-high performance concrete columns with high strength steel reinforcement. Eng Struct. 2021;232(2):111885. doi:10.1016/j.engstruct.2021.111885.
9. Guan D, Guo Z, Jiang C, Yang S, Yang H. Experimental evaluation of precast concrete beam-column connections with high-strength steel rebars. KSCE J Civ Eng. 2019;23(1):238–50. doi:10.1007/s12205-018-1807-7.
10. Khalajestani MK, Parvez A, Foster SJ, Valipour H, McGregor G. Concentrically and eccentrically loaded high-strength concrete columns with high-strength reinforcement: an experimental study. Eng Struct. 2021;248(2):113251. doi:10.1016/j.engstruct.2021.113251.
11. Li Y, Aoude H. Influence of steel fibers on the static and blast response of beams built with high-strength concrete and high-strength reinforcement. Eng Struct. 2020;221:111031. doi:10.1016/j.engstruct.2020.111031.
12. Zhang F, Feng F, Liu X. Reliability analysis of concrete beam with high-strength steel reinforcement. Materials. 2022;15(24):8999. doi:10.3390/ma15248999.
13. Du H. Experimental study on mechanical performance of HRB600 RC eccentrically loaded columns [master's thesis]. Tianjin, China: Hebei University of Technology; 2018. (In Chinese).
14. Shao X. Research on experiment behavior and calculation method of RC columns embedded with 600MPa high strength steel bars under axial and eccentric compression [master's thesis]. Hefei, China: Hefei University of Technology; 2019. (In Chinese).
15. Hung CC, Chueh CY. Cyclic behavior of UHPFRC flexural members reinforced with high-strength steel rebar. Eng Struct. 2016;122(6):108–20. doi:10.1016/j.engstruct.2016.05.008.
16. Zaky AI, El-Morsy A, El-Bitar T. Effect of different cooling rates on thermomechanically processed high-strength rebar steel. J Mater Process Technol. 2009;209(3):1565–9. doi:10.1016/j.jmatprotec.2008.04.011.
17. Krishnaa S, Veerendar C, Suriya Prakash S, Kawasaki Y. Evaluation of the fracture behaviour of concrete prisms reinforced with regular and high-strength steel rebars using acoustic emission technique. Constr Build Mater. 2023;402(5):132983. doi:10.1016/j.conbuildmat.2023.132983.
18. Xu Q, Wang J, Ding Z, Xia J, Rasa AR, Shen Q. Experimental investigation and analysis on anchorage performance of 635 MPa hot-rolled ribbed high strength rebars. Structures. 2021;30(5):574–84. doi:10.1016/j.istruc.2020.12.081.
19. Wang JH, Sun YP, Takeuchi T, Koyama T. Seismic behavior of circular fly ash concrete columns reinforced with low-bond high-strength steel rebar. Structures. 2020;27(1):1335–57. doi:10.1016/j.istruc.2020.07.005.
20. Zhang J, Liu J, Li X, Cao W. Seismic behavior of steel fiber-reinforced high-strength concrete mid-rise shear walls with high-strength steel rebar. J Build Eng. 2021;42(2):102462. doi:10.1016/j.jobe.2021.102462.
21. Sheng XW, Zheng WQ, Yang Y. Tensile and high-cycle fatigue performance of HRB500 high-strength steel rebars joined by flash butt welding. Constr Build Mater. 2020;241(6):118037. doi:10.1016/j.conbuildmat.2020.118037.
22. Code for design of concrete structures. GB50010-2010. Beijing, China: China Architecture & Building Press; 2010.
23. Chen G, Yang D. A unified analysis framework of static and dynamic structural reliabilities based on direct probability integral method. Mech Syst Signal Process. 2021;158:107783. doi:10.1016/j.ymssp.2021.107783.
24. Li L, Chen G, Fang M, Yang D. Reliability analysis of structures with multimodal distributions based on direct probability integral method. Reliab Eng Syst Saf. 2021;215(1):107885. doi:10.1016/j.ress.2021.107885.
25. Li X, Chen G, Cui H, Yang D. Direct probability integral method for static and dynamic reliability analysis of structures with complicated performance functions. Comput Meth Appl Mech Eng. 2021;374:113583. doi:10.1016/j.cma.2020.113583.
26. Tong MN, Zhao YG, Lu ZH. Normal transformation for correlated random variables based on L-moments and its application in reliability engineering. Reliab Eng Syst Saf. 2021;207(6):107334. doi:10.1016/j.ress.2020.107334.
27. Zhang XY, Lu ZH, Zhao YG, Li CQ. The GLO method: an efficient algorithm for time-dependent reliability analysis based on outcrossing rate. Struct Saf. 2022;97(12):102204. doi:10.1016/j.strusafe.2022.102204.
28. Zhang XY, Lu ZH, Zhao YG, Li CQ. Conditional time-dependent limit state function model considering damages and its application in reliability evaluation of CRTS II track slab. Appl Math Model. 2022;101(1):654–72. doi:10.1016/j.apm.2021.09.018.

29. Wang T, Li C, Zheng JJ, Hackl J, Luan Y, Ishida T, et al. Consideration of coupling of crack development and corrosion in assessing the reliability of reinforced concrete beams subjected to bending. Reliab Eng Syst Saf. 2023;233:109095. doi:10.1016/j.ress.2023.109095.
30. Tran H, Thai HT, Uy B, Hicks SJ, Kang WH. System reliability-based design of steel-concrete composite frames with CFST columns and composite beams. J Constr Steel Res. 2022;194:107298. doi:10.1016/j.jcsr.2022.107298.
31. Gauron O, Saidou A, Busson A, Siqueira GH, Paultre P. Experimental determination of the lateral stability and shear failure limit states of bridge rubber bearings. Eng Struct. 2018;174(13):39–48. doi:10.1016/j.engstruct.2018.07.039.
32. Kalfas KN, Ghorbani Amirabad N, Forcellini D. The role of shear modulus on the mechanical behavior of elastomeric bearings when subjected to combined axial and shear loads. Eng Struct. 2021;248(6):113248. doi:10.1016/j.engstruct.2021.113248.
33. Zhang W, Liu X, Huang Y, Tong MN. Reliability-based analysis of the flexural strength of concrete beams reinforced with hybrid BFRP and steel rebars. Arch Civ Mech Eng. 2022;22(4):171. doi:10.1007/s43452-022-00493-7.
34. Wang Y-H, Tian Q-L, Lan G-Q. Experimental research on the mechanical properties of concrete column reinforced with 630 MPa high-strength steel under large eccentric loading. J Jilin Univ (Eng Technol Edit). 2022;52(11):2626–35. doi:10.13229/j.cnki.jdxbgxb20210321.
35. Zhang F, Liu X, Ge FW, Cui C. Investigation on the ductility capacity of concrete columns with high strength steel reinforcement under eccentric loading. Materials. 2023;16(12):4389. doi:10.3390/ma16124389.
36. Lu R, Luo Y, Conte JP. Reliability evaluation of reinforced concrete beams. Struct Saf. 1994;14(4):277–98. doi:10.1016/0167-4730(94)90016-7.
37. Ribeiro SEC, Diniz SMC. Reliability-based design recommendations for FRP-reinforced concrete beams. Eng Struct. 2013;52:273–83. doi:10.1016/j.engstruct.2013.02.026.
38. GB 50068-2018. Unified standard for reliability design of building structures. Beijing, China: China Standard Press; 2018.
39. Zhao Y-G, Lu Z-H. Structural reliability: approaches from perspectives of statistical moments. Hoboken, NJ, USA: Wiley-Blackwell; 2021.
40. Rahman S, Xu H. A univariate dimension-reduction method for multi-dimensional integration in stochastic mechanics. Probab Eng Mech. 2004;19(4):393–408. doi:10.1016/j.probengmech.2004.04.003.
41. Huang X, Zhou Y, Li W, Hu B, Zhang J. Reliability-based design of FRP shear strengthened reinforced concrete Beams: guidelines assessment and calibration. Compos Struct. 2023;323(4):117421. doi:10.1016/j.compstruct.2023.117421.
42. Tarawneh A, Alajarmeh O, Alawadi R, Amirah H, Alramadeen R. Database evaluation and reliability calibration for flexural strength of hybrid FRP/steel-RC Beams. Compos Struct. 2024;329(6):117758. doi:10.1016/j.compstruct.2023.117758.